

A Tripole Pattern of Summertime Rainfall and the Teleconnections Linking Northern China to the Indian Subcontinent

JIE ZHANG AND HAISHAN CHEN

Key Laboratory of Meteorological Disaster, Ministry of Education (KLME), Joint International Research Laboratory of Climate and Environment Change (ILCEC), Collaborative Innovation Center on Forecast and Evaluation of Meteorological Disasters (CIC-FEMD), Nanjing University of Information Science and Technology, Nanjing, China

SIWEN ZHAO

Key Laboratory of Meteorological Disaster, Ministry of Education (KLME), Joint International Research Laboratory of Climate and Environment Change (ILCEC), Collaborative Innovation Center on Forecast and Evaluation of Meteorological Disasters (CIC-FEMD), Nanjing University of Information Science and Technology, Nanjing, China, and Fushun Meteorological Bureau, Fushun, Liaoning, China

(Manuscript received 1 October 2018, in final form 21 December 2018)


ABSTRACT

Because of the interactive margin between the East Asian summer monsoon and westerly circulation, summer rainfall in northern China (NC) exhibits high variability. By employing reanalysis data and geostationary satellite data from the *Fengyun-2G (FY-2G)* satellite and using the linear baroclinic model (LBM) and Hybrid Single-Particle Lagrangian Integrated Trajectory model, this study suggests a tripole pattern in summer rainfall over NC and the Indian subcontinent (IS) that is related to the Indian summer monsoon. The distributions of atmospheric circulation indicate three teleconnections: one is from the IS via the Indo-China Peninsula (ICP) and NC, enhancing the Pacific–Japan (PJ) pattern; another is from the IS via west-central Asia and NC, arousing a Eurasian wave pattern; and the third is an IS–TP–NC pattern via the Tibetan Plateau (TP). Those teleconnections modulate vorticity and atmospheric stability over NC. In addition, along with the circulation distribution related to those teleconnections, two pathways of moisture transport related to the IS rainfall are suggested, except for moisture transport via the Bay of Bengal: one is from the Indo-Pacific to NC due to enhancing cyclones over the Indo-Pacific and a PJ-like pattern; and another is from the IS to NC via the TP within the midtroposphere, which modulates midtroposphere moisture fluxes and atmospheric stability over NC. Both teleconnections and moisture transport result in anomalous rainfall over NC. This study reveals a new mechanism and pathway of the Indian summer monsoon impacting NC rainfall, possibly explaining the reason behind the high variability in NC rainfall.

1. Introduction

Rainfall in northern China (NC) is mainly concentrated during the midsummer, during July and August (JA), and comprises more than 50% of the annual rainfall due to moisture transport from the summer monsoon circulation; a large amount of JA rainfall is contributed by heavy rainfall events (Zhang et al. 2019). JA rainfall in NC exhibits large interannual and decadal variability; one possible reason for this variability is that

NC is a sensitive climate zone, a marginal zone between the East Asian summer monsoon (EASM) and westerly circulation (Zhang et al. 2018), which causes complex rainfall distribution. Previous studies have documented that dry/wet variability over NC strongly depends on whether EASM water vapor reaches NC and on the Pacific decadal oscillation (PDO), as well as on PDO-related sea surface temperature (SST; Qian et al. 2012; Qian and Zhou 2014). Moreover, the position of the western Pacific subtropical high (WPSH) determines the major pathway of water vapor transport toward NC and

 Denotes content that is immediately available upon publication as open access.

Corresponding author: Zhang Jie, gs-zhangjie@163.com



This article is licensed under a [Creative Commons Attribution 4.0 license](http://creativecommons.org/licenses/by/4.0/) (<http://creativecommons.org/licenses/by/4.0/>).

DOI: 10.1175/JCLI-D-18-0659.1

© 2019 American Meteorological Society

the rainfall field in NC and Japan (Tao and Chen 1987; Wu and Zhou 2008). In relation to the WPSH position, a meridional Pacific–Japan (PJ) teleconnection pattern found by Nitta (1987) also modulates EASM activity over its marginal zone, which in turn modulates dry/wet conditions over NC (Wang et al. 2015; Zhang et al. 2018). All of these results indicate that the EASM is closely related to JA rainfall in NC.

Apart from the EASM, the Indian summer monsoon (ISM) intensity exhibits strong correlations with JA rainfall in NC and southern Japan (Kripalani and Kulkarni 1997; Kripalani et al. 1997; Kripalani and Kulkarni 2001; Zhang 2001; Wang et al. 2015), and the Bay of Bengal is suggested as a key source of moisture transport linking the ISM and NC (Tao and Chen 1987); in addition, low pressure over the Indian subcontinent (IS) is also regarded as a key circulation factor (Guo and Wang 1988). Because of these linkages, some studies have discussed circulation and rainfall uniformity between the IS and NC (Liu and Ding 2008), which highlights uncertainty in the relationship of summer rainfall between the ISM and NC (Wang and Huang 2006). Moreover, the ISM tends to change in phase with the EASM (Guo et al. 2016), and El Niño–Southern Oscillation (ENSO) is considered a driving factor of phase changes in the ISM (Ashok et al. 2001). Although many efforts have been made to understand the impacts of the EASM and ISM on JA rainfall variation over NC, the multiscale and multipath impacts of complex circulation are still in need of investigation. Therefore, some other factors and mechanisms are worth discussing.

Between the IS and NC, Tibetan Plateau heating interacts with IS rainfall and the ISM, exhibiting a dipole pattern in summer rainfall across the IS and the Tibetan Plateau (Li and Yanai 1996; Xu et al. 2008; Zhou et al. 2016; Jiang and Ting 2017). Wu et al. (2012) reported that the sensible heat flux over the Tibetan Plateau is conducive to driving tropical moisture northward, which affects the position of the ISM over the IS. Summer rainfall over the southwestern Tibetan Plateau is also controlled by deep convection over the IS (Feng and Zhou 2012; Dong et al. 2016). In addition, the Tibetan Plateau heating also modulates circulation and water vapor transport over NC (Zhang et al. 2018). The question of whether the Tibetan Plateau rainfall and diabatic heating impact the rainfall relationship between the IS and NC should be addressed from an NC rainfall perspective.

Considering the high variability in NC rainfall and its complex circulation, this study focuses on the relationship between the ISM and NC in regard to JA rainfall. We attempt to understand the circulation relationships between the IS and NC to find other modulation factors impacting JA rainfall in NC.

2. Data and methods

a. Datasets

Given that more than 50% of annual rainfall and extreme events occur in JA in NC (Zhang et al. 2019), this study only analyzes JA rainfall characteristics and circulation. The reanalysis dataset of the interim daily data is from the European Centre for Medium-Range Weather Forecasts (ECMWF), with a horizontal resolution of $0.75^\circ \times 0.75^\circ$ (Dee et al. 2011; <http://apps.ecmwf.int/datasets/>). To analyze rainfall patterns, the Global Precipitation Climatology Centre (GPCC) monthly rainfall dataset from global station data from 1901 to 2016 was obtained (Becker et al. 2013), with a $1^\circ \times 1^\circ$ resolution (<https://www.esrl.noaa.gov/psd/>). To verify the results from the GPCC, we also used a monthly rainfall dataset from 1901 to 2016 from the Climatic Research Unit (CRU; version 4.01, $0.5^\circ \times 0.5^\circ$ grid, <http://catalogue.ceda.ac.uk/uuid/>). GPCC agrees well with observations precipitation in Asia, while CRU datasets agree less well (Wang and Wang 2017).

The *Fengyun-2G* (*FY-2G*) stationary satellite was launched on 31 December 2014 and was located at 105°E on 1 July 2015. It provides five bands of measurements, including one visible band ($0.55\text{--}0.75\ \mu\text{m}$) at 1.25-km resolution, one middle infrared band ($3.5\text{--}4.0\ \mu\text{m}$), two thermal infrared bands ($10.3\text{--}11.3$ and $11.5\text{--}12.5\ \mu\text{m}$), and one water vapor band ($6.3\text{--}7.6\ \mu\text{m}$) at a 5-km resolution. Several atmospheric products from the *FY-2G* data have been developed for weather monitoring and predictions; for example, the atmosphere motion vector in the upper-middle and lower troposphere can be determined, with a speed bias of $0.48\ \text{m s}^{-1}$ (Yang et al. 2014). The total precipitable water vapor has been corrected and improved due to reducing retrieval errors caused by surface emissivity uncertainties and observation errors, especially under drier atmospheric conditions where the total precipitable water vapor is less than 2 cm (Liu et al. 2017).

b. Models and other methods

The linear baroclinic model (LBM) is used to simulate atmospheric response to an idealized forcing of diabatic heating over the IS. The LBM has a triangular truncation of 21 waves and a vertical resolution of 20 levels (Watanabe and Kimoto 2000). The experiment background state is the mean JA climatology from 1979–2016, obtained from ECMWF interim reanalysis (ERA-Interim) data; the forcing center is over 25°N , 80°E , with a horizontal scale of 20° longitude and 10° latitude; the vertical forcing is at 500 hPa; the integration time for the model is set to 31 days, because simulated circulation response to forcing could approach the steady state after the 15th day; and the

data during days 15–30 could be used for analyzing circulation characters.

The Hybrid Single-Particle Lagrangian Integrated Trajectory model (HYSPPLIT) is a complete system for computing simple water vapor transport and other transport and deposition simulations (Stein et al. 2015). The HYSPPLIT trajectory is used for investigating of water vapor trajectories, with consideration to both forward and backward trajectory directions. The details of the HYSPPLIT trajectory model can be found on the website <https://ready.arl.noaa.gov/HYSPPLIT.php>. To overcome the uncertain problems of Lagrangian trajectory and moisture releasing as rainfall before it arrives at the target position, Sodemann et al. (2008) developed a method based on the Lagrangian trajectories. Hereafter, Huang et al. (2018) recently presented a comprehensive summary of Sodemann et al. (2008) and defined a concept “characteristic trajectory” for the moisture transport from one region to the target region. Based on those two improved methods, the study verifies that the Lagrangian trajectory could deliver moisture between those two regions.

The wave activity flux (WAF) is a useful diagnostic method for illustrating stationary or migratory quasi-geostrophic wave disturbances and for revealing where anomaly waves are emitted, absorbed and transferred (Takaya and Nakamura 2001), and the wave flux is therefore defined as TNF. An empirical orthogonal function (EOF) analysis is applied to the temporal correlation matrix of JA rainfall. A regression is used to investigate the relationship of JA rainfall to the ISM and anomalous circulation. A synthesis analysis is used to examine rainy-day circulation, moisture fluxes, and satellite data. Based on EOF analysis, two regions representing Indian precipitation and NC precipitation are defined, namely the IS (18°–32°N, 66°–90°E) and NC (37°–44°N, 105°–120°E).

3. Results

a. The tripole pattern in summertime rainfall

Figure 1a shows the first leading mode (shaded) of JA rainfall anomaly. The mode exhibits a tripole pattern between the IS and NC, with high negative anomaly centers over the IS and NC and one positive anomaly center over the eastern Tibetan Plateau. A reverse rainfall distribution between the IS and the Tibetan Plateau has been discussed by Jiang and Ting (2017), but available studies on the reverse rainfall distribution between the Tibetan Plateau and NC are limited. In addition, rainfall over southern China and the Indo-China Peninsula (ICP) show a similar pattern as observed over NC and the IS. The ICP–NC distribution

is also a tripole-like pattern and is potentially linked with the PJ pattern (Nitta 1987). The above rainfall distribution reveals that NC rainfall has potential linkages with rainfall over ICP and IS, although the variance of EOF modes is low in our study region, which includes different rainfall climate zones and complex circulations. The coincidental distribution of rainfall over the IS and ICP is possibly related to the interaction between the ISM and EASM (Guo et al. 2016). The PJ wave train begins from the tropical western Pacific Ocean and is related to convective heating anomalies, that is, in response to the PDO-associated warm SST anomalies over the tropical western Pacific Ocean (Qian and Zhou 2014) and the tropical Indian Ocean (Hu et al. 2011); therefore, the anomaly of PJ patterns could explain NC rainfall changes and the relationship with tropical oceans and circulations. Figure 1b shows the first leading principal component (PC), which indicates a decadal variability with negative anomalies before 1960 and after 2000 and positive anomalies between 1960 and 2000.

To demonstrate the multiscale rainfall variability over the IS and NC, temporal variations of JA rainfall over the IS and NC are shown in Fig. 1c. The central rainfall over the IS region coincides with the ISM zone and is highly correlated with variations in Indian summer rainfall. Therefore, the central rainfall over the IS is widely used to measure rainfall variations in the ISM (Gadgil 2003), and normalized JA rainfall over the IS region is defined as the ISM index. PC1 shows a high correlation with ISM, with a correlation coefficient of -0.51 (Fig. 1b). Using the ensemble empirical mode decomposition (EEMD) method (Wu and Huang 2009), the multiscale variations of rainfall over the IS and NC are investigated. Both JA rainfall variations over the IS and NC are significantly correlated on an interannual scale with a 2- to 3-yr period (Fig. 1c, panel 1), on an interdecadal scale with a 5- to 7.1-yr period (Fig. 1c, panel 3), and on a multidecadal scale with more than a 10-yr period (Fig. 1c, panel 4), but the relationship of the interannual scale with a 3.1-yr period (Fig. 1c, panel 2) is weak; the best relationship is on the interdecadal scale, indicating multiscale rainfall relationships between the IS and NC. The correlation between the IS and NC at interannual and interdecadal scales could be explained by IS–tropical Pacific–ICP–NC relationship. The relationship at the multidecadal scale could be explained by an SST pattern in the Indian and Pacific Oceans with a PDO phase change (Qian and Zhou 2014), which induces the PJ pattern linking NC rainfall, through a Kelvin wave response to ISM-related convective heating, and the conduction of an anticyclone over the Philippine Sea and a cyclone ICP, which contributes PJ patterns and NC rainfall at the interannual time scale

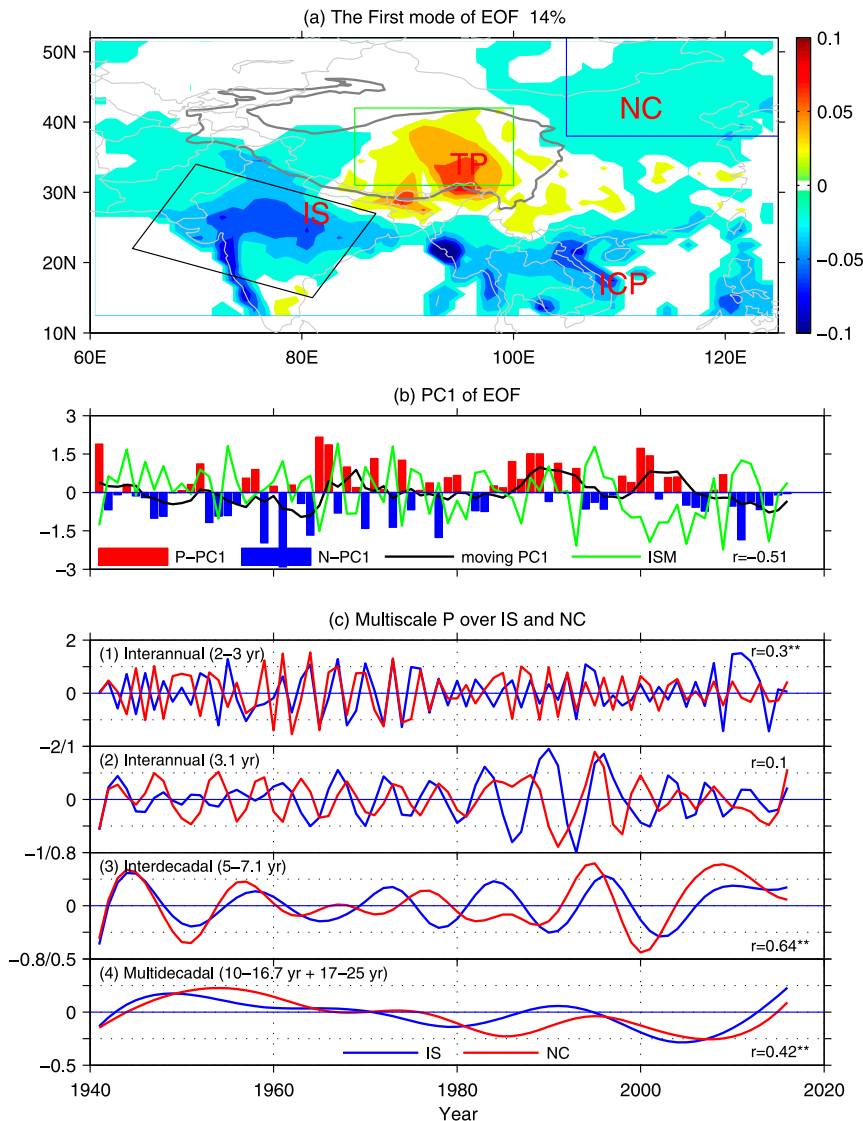


FIG. 1. (a) The first leading mode of the JA rainfall EOF (shaded) and (b) the related first principal component from the GPCC, and (c) JA rainfall series over the IS and NC regions on different time scales. One asterisk (*) represents a 95% confidence level, and two asterisks (**) represent a 99% confidence level. Rectangles are study regions including IS, NC, and TP.

(Wu et al. 2009); however, increases of ISM-related convective heating over the Indian Ocean induce local Hadley circulation and cause anomalous subsidence near the Philippines, further impacting PJ patterns and NC rainfall at the interdecadal time scale (Hu 1997). A previous study has indicated that this dissimilarity at the 3.1-yr scale is possibly related to the ENSO (Ashok et al. 2001), and another key reason for this dissimilarity is that the IS rainfall is impacted by the ISM; however, NC rainfall is impacted not only by the ISM but also by the westerly and the EASM (Kripalani and Kulkarni 2001). In all, apart from PDO effects, the above analysis

indicates the main relationship between the ISM and NC at interannual and interdecadal time scales.

To further exhibit the JA rainfall relations between NC and the IS at the interannual and interdecadal time scales, a regression of JA rainfall in relation to the ISM index and a regression with the multidecadal movement are shown in Fig. 2. The figure indicates two significant tripole patterns: the first is the IS–NC pattern via the Tibetan Plateau, which is similar to the first pattern of the EOF analysis for JA rainfall. The second is the ICP–NC pattern linking southern China and NC, which is similar to a westward-extending PJ pattern. Both

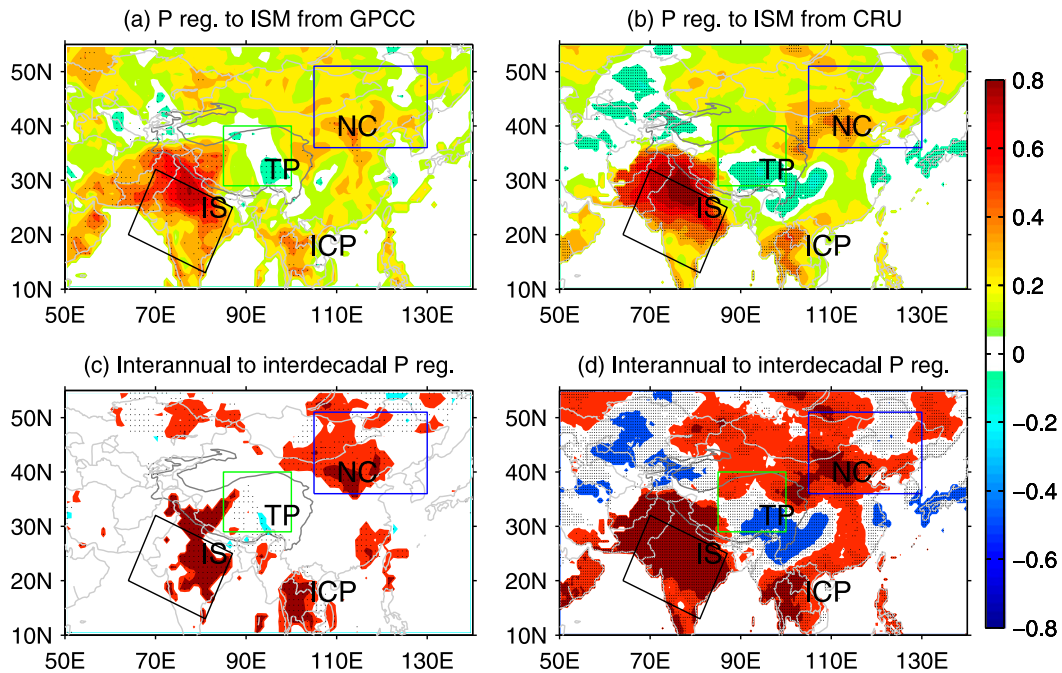


FIG. 2. JA rainfall regression to the ISM index from (a) the GPCC dataset and (b) the CRU dataset, as well as interannual and interdecadal JA rainfall regression to the interannual and interdecadal ISM indexes from (c) the GPCC dataset and (d) the CRU dataset. The dots represent the 95% confidence level.

patterns from the two datasets are similar, indicating that they may be related to JA rainfall over NC and that multipath circulation impacts NC rainfall. Additionally, JA rainfall distributions over the IS and the ICP are highly correlated, which means that the ISM and EASM interactions are impacted by other circulation patterns and forces. In addition, a similar trend between the IS and NC is possibly related to the PJ-like pattern. Although the ICP–NC pattern and the related EASM are dominant factors impacting NC rainfall (Kripalani and Kulkarni 2001; Hsu and Lin 2007) and the ISM impacts NC rainfall by moisture transport across the Bay of Bengal (Tao and Chen 1987), the IS–NC tripole pattern results in a new pathway that could modulate NC rainfall. We explore how the IS–NC tripole pattern impacts NC rainfall in the next section.

b. The relationships between circulation and the tripole patterns of rainfall

To explain the linkage between NC rainfall and the IS–NC tripole pattern, the circulation character is investigated. Given that the tripole pattern links NC, the Tibetan Plateau, and the IS, rainfall and circulation in these regions are closely related to the summer monsoon, diabatic heating of the Tibetan Plateau, and the ISM, which exhibit quasi-biweekly and other scale oscillations (Li et al. 2011) and which could contribute to

monthly and interannual variation of JA rainfall. Based on this information, the 10-day mean circulation in JA is investigated to highlight circulation patterns related to the rainfall's tripole pattern. Figure 3a shows the first leading mode of the 10-day vorticity in JA (shaded), and the vorticity mode exhibits a tripole pattern between the IS and NC. The figure also shows a highly negative anomaly centered over the IS and NC and a positive anomaly centered over the eastern Tibetan Plateau. The reverse vorticity distribution between the IS and the Tibetan Plateau is in accordance with the rainfall pattern (Jiang and Ting 2017). The tripole pattern of the vorticity over southern China and NC is similar to the PJ rainfall patterns shown in Fig. 1. Figure 3b shows the leading PC, and its monthly mean value is positively correlated with the IS monsoon index with a correlation coefficient of 0.37, as tested by the Monte Carlo method. This indicates the interannual and interdecadal variability and explains the tripole rainfall pattern.

To further demonstrate how the circulation distribution corresponds to the JA vorticity pattern, an anomalous circulation regression is shown in Fig. 4a. The figure indicates two significant tripole patterns linking NC climate and the vorticity patterns in Fig. 3 and rainfall patterns in Fig. 1. One of these tripole patterns is the IS–NC pattern via the Tibetan Plateau; the other is the ICP–NC pattern. The results indicate that the

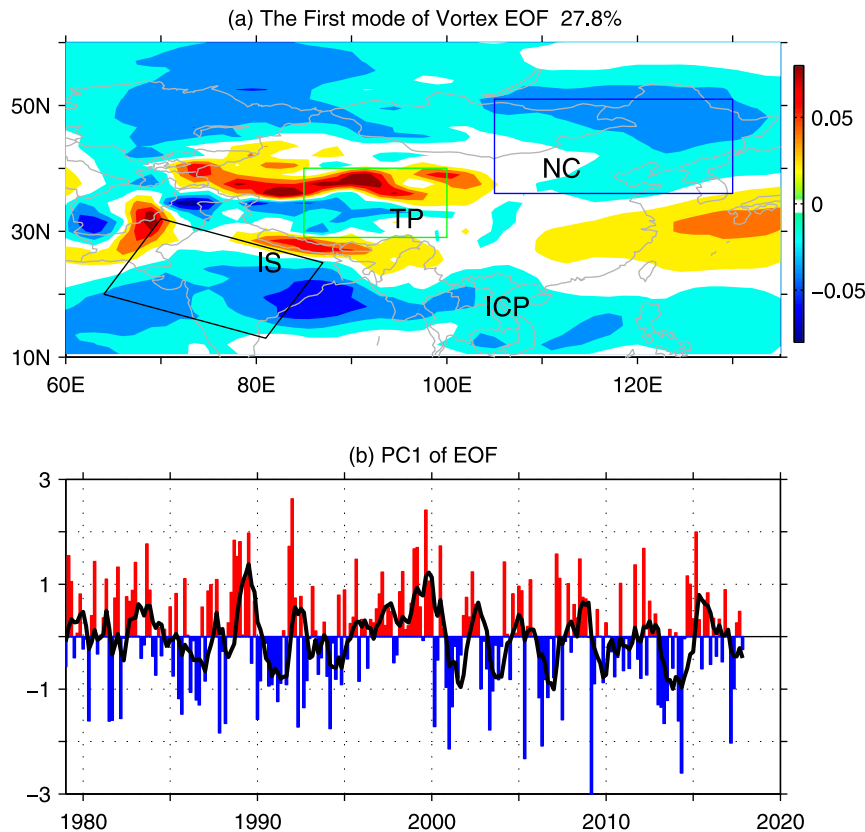


FIG. 3. (a) The first leading mode of the 10-day vorticity EOF (shaded) and (b) the related first principal component (PC1), and a 6-point (1 yr) running mean PC1 (black line).

circulation anomalies over NC link to two teleconnection-like patterns, which are the primary reasons why there are two tripole patterns and a coincident variety of circulation and rainfall over NC, IS, and ICP. Because decadal trends are not removed, the regression also includes the PDO effect. The study also conducts a regression with removing decadal trends, and the spatial distribution of circulation is similar to Fig. 4a, which indicates that two patterns also occur at the interannual and interdecadal time scale.

To demonstrate the role of these teleconnection-like patterns, wave motion flux was regressed to the first leading PC of the vortex (Fig. 4b). In addition to significant zonal wave motion flux over the midlatitudes, three branches of meridional wave motion fluxes are clear. One branch shows that the primary distribution of the wave motion flux is from the ICP to NC, exhibiting ICP–NC (see green arrow) and PJ-like patterns; another branch is weaker, along the IS–NC pattern (see red arrow). Both branches of wave motion flux show that wave energy could be transported along the IS–NC and the ICP–NC teleconnections, contributing kinetic energy and circulation configuration. The wave motion

flux from the IS toward the northwest of the Tibetan Plateau is also suggested by Huang et al. (2015a,b). In addition, zonal wave motion flux over the midlatitudes spans from the IS and the Arabian Sea and via an energy-sinking region over west-central Asia toward East Asia, which could enhance circulation over western and central Asia that modulates the midlatitude Silk Road wave train (Ding and Wang 2005; Yang et al. 2009) and further modulates circulation over NC and Japan (Krishnan and Sugi 2001; Zhang et al. 2018); therefore, it is possible that through the third teleconnection pattern, a circulation anomaly over the IS could also impact NC circulation. The wave motion flux distribution (Fig. 4b) is similar to the regression of the rainfall PC (figure omitted). In all, the tripole rainfall pattern is related to the tripole circulation and the wave energy transportation of teleconnections, indicating the impact of the multipath circulations on NC rainfall.

c. The relationship between the moisture flux and teleconnection patterns in August 2016

Given the multiscale rainfall relations between the IS and NC, and the circulation uncertainties of

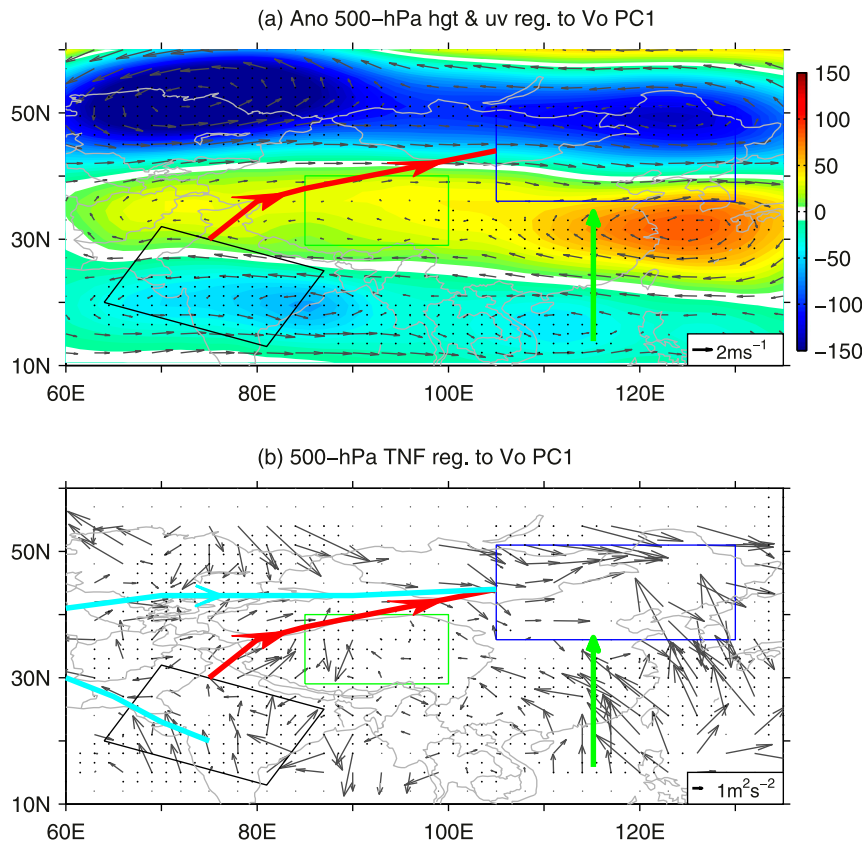


FIG. 4. (a) Anomaly geopotential height (shaded; gpm) and flow field (velocity) regression to the 10-day vortex PC1 and (b) wave motion flux regression to the 10-day vortex PC1 in JA. The dots represent the 95% confidence level, and the red, blue, and green arrows represent TNF directions.

reanalysis datasets around the Tibetan Plateau (Zhu et al. 2012), we mainly focus on interannual relationships of circulation in this study to contrast the reanalysis results with satellite results. To further explore how the IS–NC tripole pattern modulates NC rainfall, we analyzed circulation, moisture flux, and moisture flux divergence from 15 to 25 August 2016. The reason to select this period is that analysis excludes two events in August with tropical cyclones and typhoons, which have led to heavy rainfall in NC; in addition, Chinese forecasters failed to forecast the heavy rainfall events from 10 to 25 August 2016, including two selected heavy rainfall cases from 15 to 25 August. The synthetic analysis of geopotential heights and wind velocities at 500 hPa (Fig. 5a) indicates that there are two teleconnection patterns. The first pattern is an IS–NC tripole pattern, with a cyclone over the IS and a trough over NC, but with an anticyclone anomaly over the eastern Tibetan Plateau to the subtropical western Pacific. This pattern coincides with rainfall patterns over NC and the IS, revealing a teleconnection pattern. The wind velocity

at 500 hPa indicates a direct relationship between the IS and NC climate via the Tibetan Plateau. The second teleconnection pattern is the ICP–NC tripole pattern, which exhibits a cyclone over the ICP to the western Pacific and a trough over NC, but with an anticyclone along the Yangtze River. Contrasting circulation patterns over the IS and ICP indicate that the cyclones over the two regions are not only isolated but also connected by the west-extending WPSH (Fig. 5a). Easterlies on the southern side of the WPSH are conducive to moisture transport, and a cyclone over the ICP and western Pacific propagating toward the IS enhances the cyclone anomaly over the IS and the northward flow via the Tibetan Plateau toward NC.

These teleconnection patterns only show the circulation relationships between the IS and NC. To further reveal the relationships between rainfall and teleconnection patterns, moisture flux and moisture flux divergence from the surface to 600 hPa (Fig. 5b) and from 600 to 300 hPa (Fig. 5c) are used to reflect moisture distribution in the lower troposphere and above the

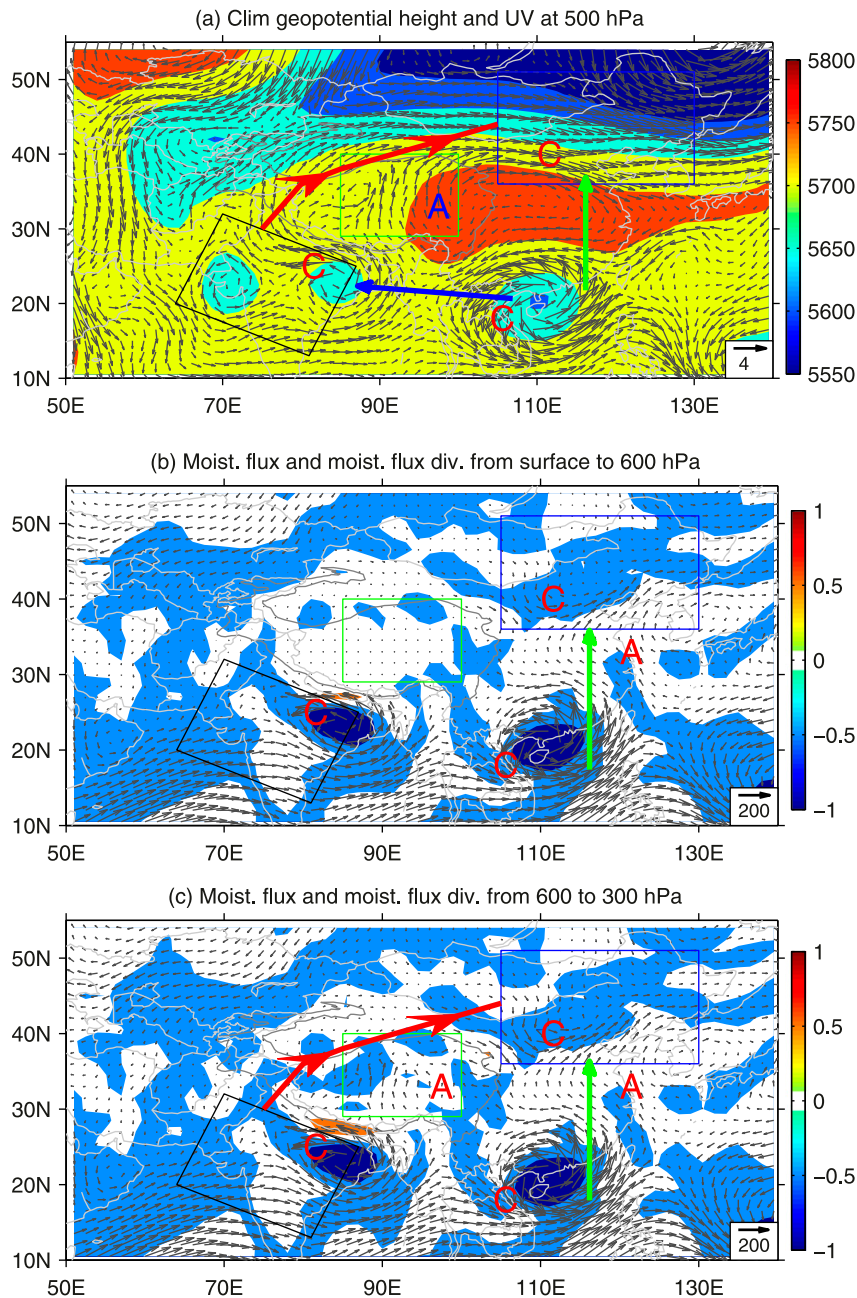


FIG. 5. (a) Climatological geopotential heights (gpm) and wind velocities (m s^{-1}) at 500 hPa, and moisture flux ($\text{kg m}^{-1} \text{s}^{-1}$) and moisture flux divergence ($10^{-5} \text{kg m}^{-2} \text{s}^{-1}$) (b) from the surface to 600 hPa and (c) from 600 to 300 hPa from 15 to 25 Aug 2016. Letters A and C indicate anticyclone and cyclone, respectively. Red and green arrows are as in Fig. 4.

height of the Tibetan Plateau. Moisture divergence also indicates the convergence over the IS, NC, and ICP, corresponding to rainfall over these three regions (Figs. 1 and 2). Figure 5 indicates that the ICP–NC pattern is very deep because it appears from the surface to the upper-middle troposphere, and it causes a significant moisture flux over NC. The moisture flux is also

isolated over the IS and ICP, and moisture transportation extends westward from the ICP and western Pacific to the IS, which is similar to the results shown in Fig. 5a. Because of the high altitude of the Tibetan Plateau, with an average height of 4000 m, the moisture flux from the IS region could be concentrated in the upper-middle troposphere. Although there is a decrease

in the moisture flux along the IS–NC path, it is still an important consideration for NC rainfall because it could modulate the midtroposphere moisture and atmospheric stability. These results indicate that ICP–NC circulation pattern contributes major moisture fluxes to NC; in addition, the IS–NC circulation teleconnection could contribute to the midtroposphere moisture flux to NC and should be a significant contributor to NC rainfall because it could modulate moisture distribution and atmospheric stability. However, a quantitative evaluation of the IS–NC tripole pattern and teleconnection is still necessary to confirm these results.

d. Teleconnection patterns and water vapor distribution from the FY-2G satellite

As discussed above, the teleconnection explains the IS–NC tripole pattern and the related moisture flux over NC. However, due to high topography and complex land surfaces, the reanalysis datasets and simulations exhibit high uncertainty, especially over the Tibetan Plateau (Zhu et al. 2012). To further demonstrate the impacts of the IS–NC tripole pattern and teleconnection on NC rainfall, we employ products from the Chinese geostationary satellite *FY-2G* to explore the moisture flux and water vapor content throughout the upper-middle troposphere. Figure 6 shows the distribution of atmospheric motion vectors using the infrared water vapor band (IR3) from the *FY-2G* satellite and upper-middle tropospheric humidity (Fig. 6a), total precipitable water vapor (Fig. 6b), and outgoing longwave radiation (Fig. 6c).

Atmospheric motion vectors from the infrared water vapor band indicate westward cloud propagation from the ICP to the IS, which is similar to the circulation and moisture flux motions discussed in Fig. 5. In addition to the IS–NC tripole pattern and teleconnection, there are significant moisture movements toward NC over the Tibetan Plateau that are similar to the circulation patterns and moisture fluxes mentioned previously, but the motion velocity is larger than that calculated from the reanalysis data. This result not only exhibits the uncertainties in the reanalysis, but it also indicates that moisture and clouds in the upper-middle troposphere could be transported along the IS–NC teleconnection, and their contribution to NC rainfall exceeds our expectations and reanalysis results. Moisture motion along the ICP–NC pathway is weaker than it is along the IS–NC pathway. One possible reason is that the infrared band of the satellite is unable to obtain moisture information in the lower troposphere. Another possible reason is that the ICP–NC pattern throughout the upper-middle troposphere is weak. Overall, atmospheric motion vectors could indicate IS–NC and ICP–NC

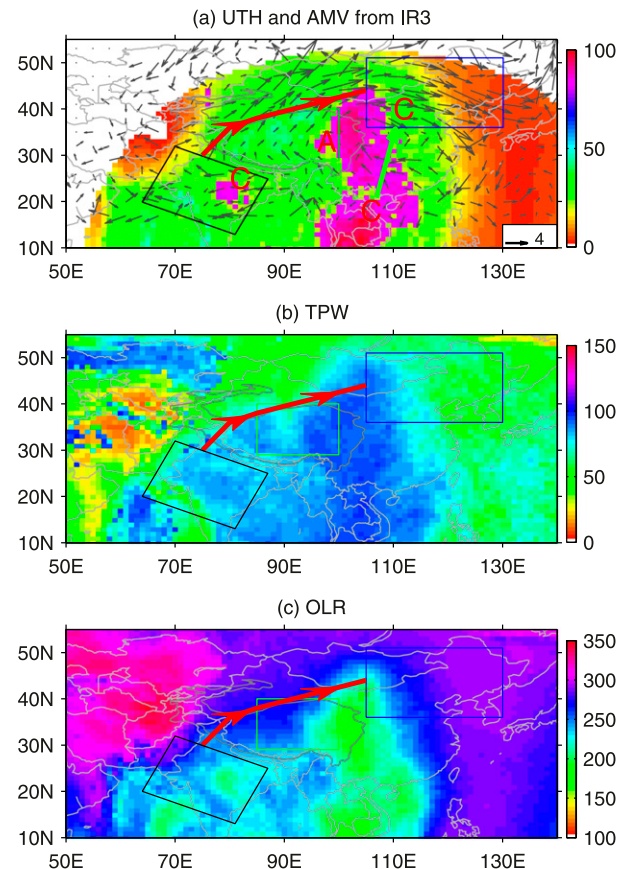


FIG. 6. (a) Distribution of atmospheric motion vectors from IR3 (m s^{-1}) and upper-middle tropospheric humidity (%), (b) total precipitable water vapor (mm), and (c) outgoing longwave radiation (W m^{-2}) from 15–25 Aug 2016 from the *FY-2G* satellite. Letters A and C indicate anticyclone and cyclone, respectively. Red and green arrows are as in Fig. 4.

teleconnections, with the moisture transport from the ICP to the IS. These results are consistent with those depicted in Fig. 5. Upper-middle tropospheric humidity indicates that large amounts of humidity are concentrated between 50° and 120°E over the tropics, but between 70° and 120°E over other Asian regions. The most significant region is along 105°E from the ICP to NC, which is possibly related to the ICP–NC pattern and moisture flux from the Bay of Bengal. The secondary center is along the IS–NC pathway, which implies that a moisture flux exists over the Tibetan Plateau.

To further show the importance and concentration of the moisture flux along these two teleconnection pathways, especially the moisture flux along the IS–NC pathway, total precipitable water vapor and outgoing longwave radiation are analyzed. Similarly, the upper-middle tropospheric humidity and total precipitable water vapor are largely distributed along the ICP–NC

pathway and exhibit a secondary region along the IS–NC pathway from the IS to the north of the Bay of Bengal. The average moisture flux is as high as 70% of that seen along the ICP–NC regions, and due to high moisture content and precipitable water vapor, this result indicates that the IS–NC is a new pathway for moisture transport over NC. Given the limitations of the reanalysis data, this pathway had not been discovered prior to this study.

Outgoing longwave radiation is one of the most important components in the global energy balance of the Earth–atmosphere system and is determined mainly by emission temperatures. Because it can exhibit cloud top temperatures under a cloud-covered sky, outgoing longwave radiation is used to compare cloud cover, radiation and convection characteristics. Figure 6c indicates that outgoing longwave radiation exhibits low values along the ICP–NC due to high cloud cover in response to rich moisture fluxes and moisture convergence conditions. The region from the IS to the Tibetan Plateau is a secondary radiation region, with low outgoing longwave radiation and relatively high cloud cover. However, the longwave radiation is slightly higher over the central Tibetan Plateau, which is different from the distribution of precipitable water vapor and upper-middle tropospheric humidity because it is related to high surface temperatures.

Results from the satellite data indicate that the IS–NC tripole pattern for JA rainfall is related to the teleconnection and moisture flux along the IS–NC, but its contribution to NC rainfall is related to ICP–NC and moisture fluxes across the Bay of Bengal. The teleconnection links cyclones over the IS and anticyclones over the Tibetan Plateau and exhibits a trough over NC. Thus, the teleconnection clearly corresponds to those circulation variations, especially for the anticyclone that exhibits a westward-extending WPSH anomaly. This teleconnection not only leads to the westward transportation of moisture fluxes and cyclones from the ICP to the IS but is also responsible for northward moisture transportation from the IS via the Tibetan Plateau toward NC. Therefore, WPSH is a possible factor driving the IS–NC teleconnection and tripole pattern. In addition, the IS cyclone is also an important factor. Why the WPSH exhibits a westward-extending anomaly and what causes the IS cyclone variations are important questions for understanding the IS–NC teleconnection, and these issues will be discussed in the next study.

Figure 7 shows an animation of the atmospheric motion vectors from the infrared water vapor band and upper-middle tropospheric humidity for eight consecutive days (17–24 August 2016) within 15–25 August, as the period includes two heavy rain events in NC that

were not influenced by tropical systems including typhoons, and those cases could exhibit the contributions of teleconnections and moisture transport pathways. Upper-middle tropospheric humidity indicates that the significant region is along 105°E from the ICP to NC and that it is the most significant moisture transport, relating to EASM circulation and a JP-like pattern. In addition, Fig. 7 also indicates consecutive moisture transport along the IS–NC with a secondary center, and there is significant moisture transport over the Tibetan Plateau toward NC with an anticyclonic trend, similar to the circulation and moisture fluxes mentioned previously. The results demonstrate two branches of significant moisture transport toward NC, especially moisture transport via the Tibetan Plateau. In addition, the moisture transport also shows a westward movement of moisture from the ICP to the IS along the westerly on the south side of the WPSH and along the north Indian Ocean; the eastward moisture moves from the IS to the ICP along southwesterly of cross-equatorial flows, indicating their interaction.

e. Linking the tripole patterns and teleconnections to NC rainfall

Using the backward trajectory simulation of the HYSPLIT model (Fig. 8, right panel), NC water vapor was investigated at 0000 UTC within 10 days, 15–25 August 2016, and the cases include 131 792 air particles. The results show three branches of water vapor pathways: the first pathway comes from the southern and western Pacific and is mainly transported by EASM circulation, linking to a PJ pattern and the WPSH (Tao and Chen 1987; Kripalani et al. 2001); it is generally the major pathway of moisture transport, but it is weak during our selected period. The second pathway is along the westerly in the midlatitudes (Zhang et al. 2018), and the third pathway is via the Tibetan Plateau and the IS. To confirm the third pathway, we conducted a forward trajectory simulation of the HYSPLIT model, and the cases included 120 441 air particles. By defining a water vapor source over the northwest IS (Fig. 8, left panel), water vapor is transferred in two directions: one branch is southward and westward, and the other branch is northward, via the Tibetan Plateau and toward NC. This pathway agrees with the backward trajectories of water vapor over NC, which further confirms a moisture transport from the IS toward NC. The distribution height of water vapor included mid- to upper levels and lower levels to NC, and the water vapor from the IS toward NC is from the mid- to upper levels, as it reaches 400 hPa over the Tibetan Plateau. However, more than half of water vapor could reach the middle and lower levels over NC, with decreasing altitude, which is in the

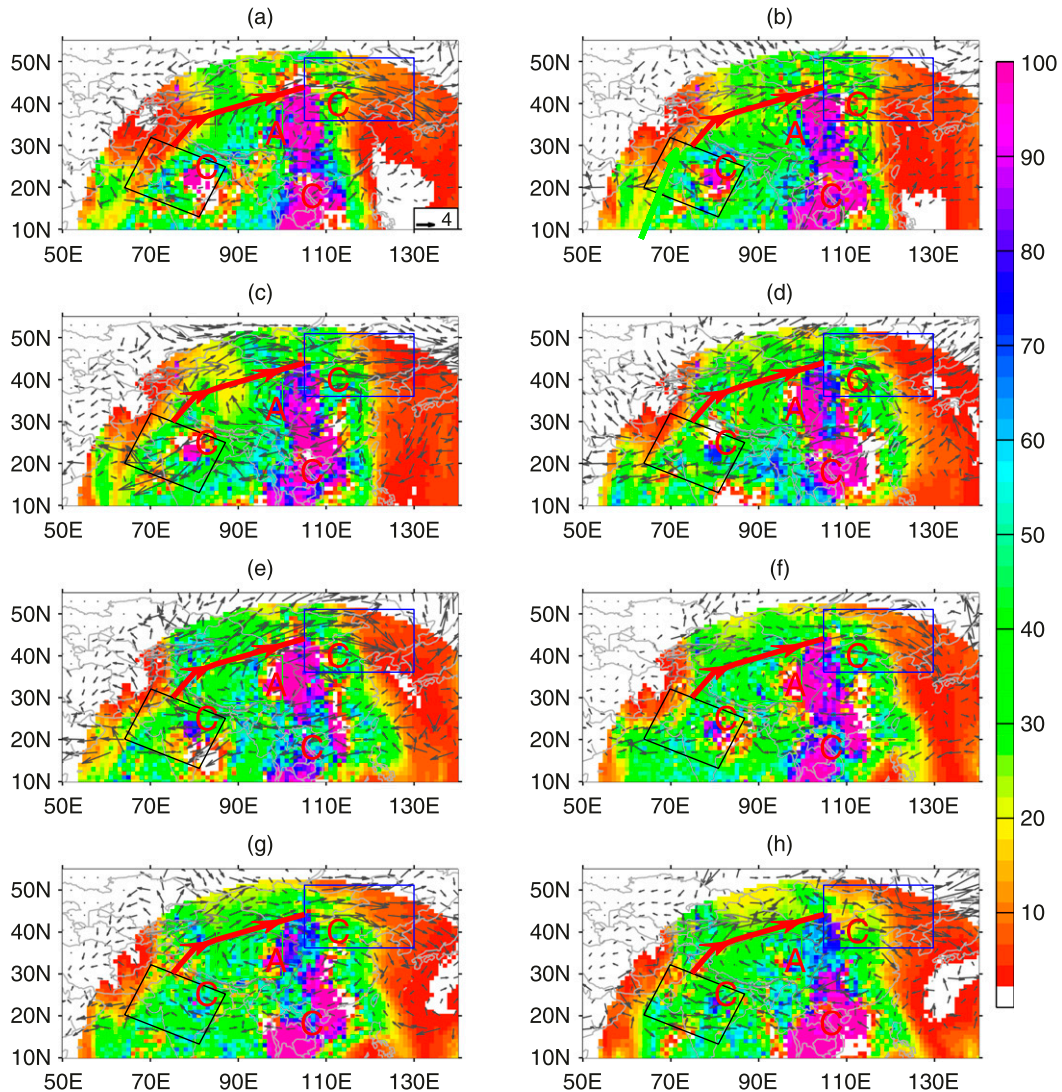


FIG. 7. Animated distribution of atmospheric motion vectors during eight consecutive days (within the period 15–25 Aug 2016) from IR3 (m s^{-1}) and upper-middle tropospheric humidity (%) from the *FY-2G* satellite. Letters A and C indicate anticyclone and cyclone, respectively. Red and green arrows are as in Fig. 4.

ascending motion and efficient level of rainfall. Therefore, it encourages rainfall. How this mid- to upper-level water vapor contributes to NC rainfall requires further evaluation.

The two basic conditions of moisture flux and ascending vertical motion for moisture convergence and rainfall are investigated by using specific humidity and vertical velocity, respectively (Fig. 9), to understand the contribution of the IS–NC teleconnection and circulation to NC rainfall. Vertical distribution of vertical velocity along a meridional profile (110° – 115°E) over NC shows that although the mean vertical velocity is larger than zero above 400 hPa (Fig. 9a), it is still less than zero from the surface to 400 hPa for many cases.

This result denotes a significant vertical motion that could lead to rainfall if there is enough water vapor. The vertical distribution of a specific humidity along the western profile (35° – 45°N , 95° – 96°E ; Fig. 9b) exhibits a specific humidity larger than 5 g kg^{-1} from the surface to 600 hPa, and it mainly includes water vapor along the IS–NC, which in combination with the vertical velocity and specific humidity could lead to significant rainfall (Li et al. 2012). To compare the different contributions of the IS–NC pattern and the EASM from the western and tropical Pacific, the vertical distribution of vertical velocity (Fig. 9c) and specific humidity (Fig. 9d) along a zonal profile (100° – 125°E) over the southern side of NC is investigated. The mean vertical velocity over the

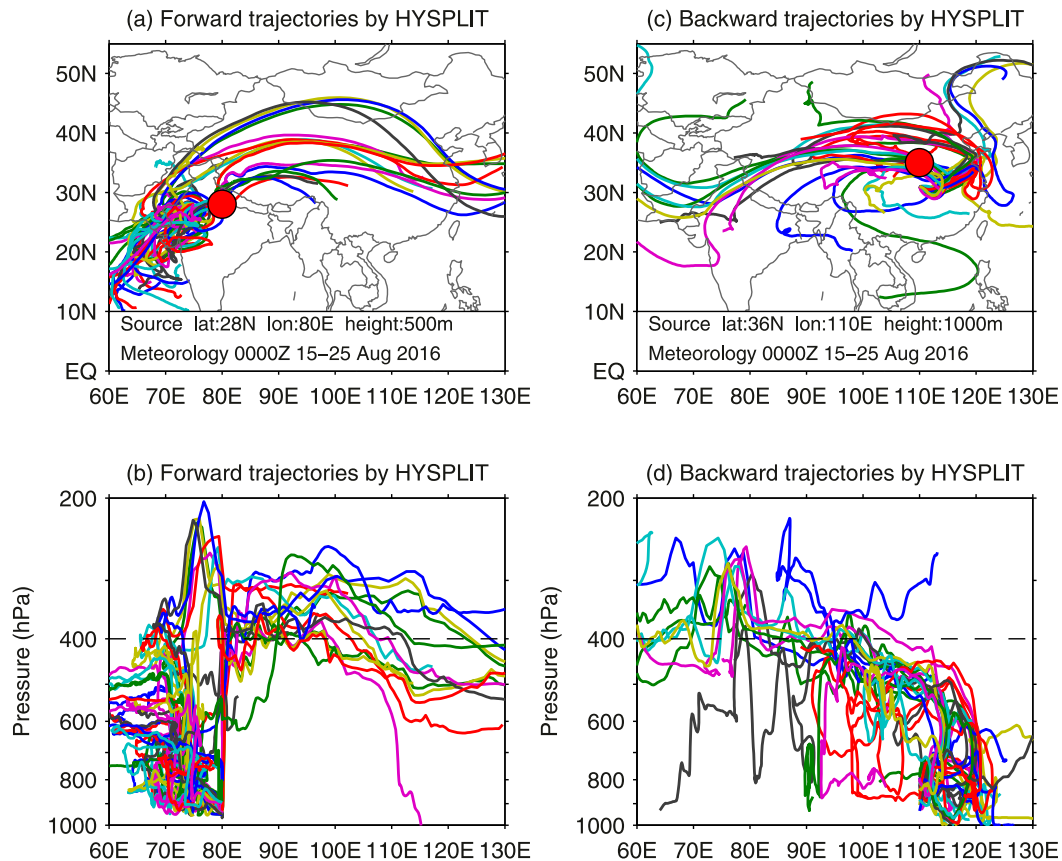


FIG. 8. (right) The source of water vapor over NC at 0000 UTC over 10 days (15–25 Aug 2016) obtained from backward trajectories and (left) the forward moisture transport over IS obtained from forward trajectories from the HYSPLIT model.

southern side is larger than that over the western profile, and the ascending motion reached 600 hPa, but the variability and maximum of ascending motion depth are less than those along the meridional profile over NC. The vertical distribution of specific humidity is larger than that along the meridional distribution below 700 hPa but is less than that from 700 to 500 hPa. The results indicate that EASM from the southern part of NC mainly contributes lower-middle moisture to NC; however, the IS–NC pathway mainly contributes upper-middle moisture. Due to a deep ascending motion over NC, moisture transport along the IS–NC pathway could be a partial contributor to NC rainfall. In addition, IS–NC teleconnection could modulate circulation, humidity, and vertical motion over NC, which further modulates NC rainfall.

f. The mechanism of the Indian monsoon effect on the tripole pattern

The tripole pattern of rainfall and circulation corresponds to the IS–NC teleconnection. Therefore, related

circulation systems are important for tripole patterns. The IS–NC tripole pattern is closely related to the IS cyclone. In this section, we simulated the IS cyclone and rainfall anomaly by strengthening diabatic heating over the IS. The LBM is used to simulate the atmospheric response to an idealized forcing of condensation diabatic heating. The background data are the JA means from 1979 to 2017 from ERA-Interim. The 4-day circulation evolution within 16 days is investigated because atmospheric response reaches equilibrium by the 16th day.

Figure 10 shows the geopotential height and wind velocity anomaly every four days. A cyclone anomaly forms over the IS, which gradually progresses circulation anomalies toward the northeast, and an anticyclone anomaly appears over the eastern Tibetan Plateau, which gradually amplifies toward northwest China. Finally, a negative–positive–negative (–+–) IS–NC pattern appears on the eighth day, with a cyclone anomaly over the IS and NC and an anticyclone anomaly over the eastern Tibetan Plateau, which agrees with the above diagnostic analysis on the climate and

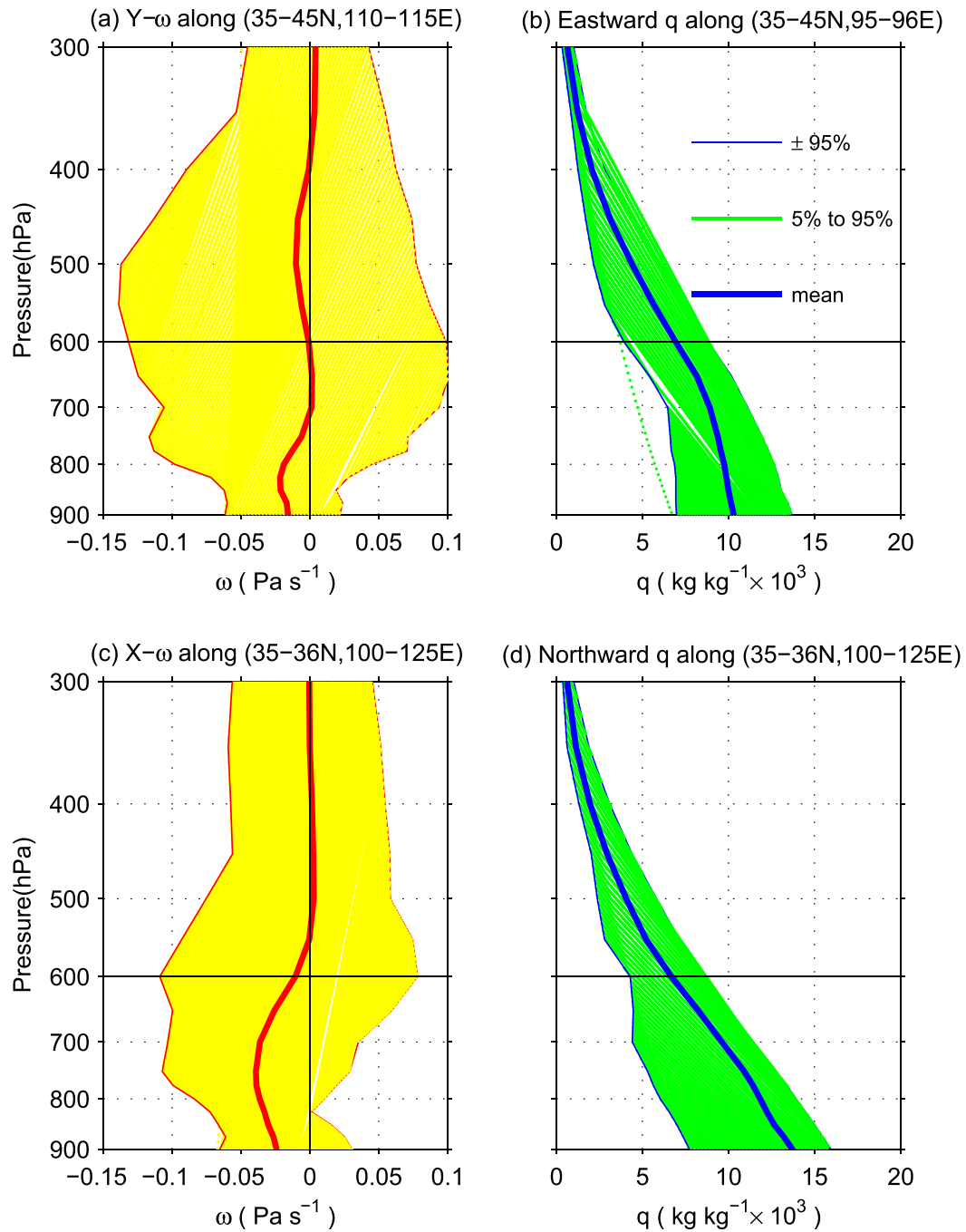


FIG. 9. (a) Vertical distribution of the vertical velocity along the meridional profile (110°–115°E) over NC, (b) specific humidity along the western profile (35°–45°N, 95°–96°E), (c) vertical distribution of vertical velocity, and (d) specific humidity along the zonal profile (100°–125°E) over the southern side of NC over 10 days (15–25 Aug 2016).

weather scale. The simulation reveals that a circulation anomaly over the IS could contribute to the IS–NC teleconnection, which contributes to an increase in ascending motion over NC and the tripole rainfall pattern. Other circulation patterns, such as the anticyclone

anomaly over the eastern Tibetan Plateau, are also significant and should be addressed. With circulation evolution, a $-+-$ pattern from west-central Asia to NC is clear, indicating another teleconnection linking with IS cyclone. In addition, a cyclone over the Indo-Pacific is

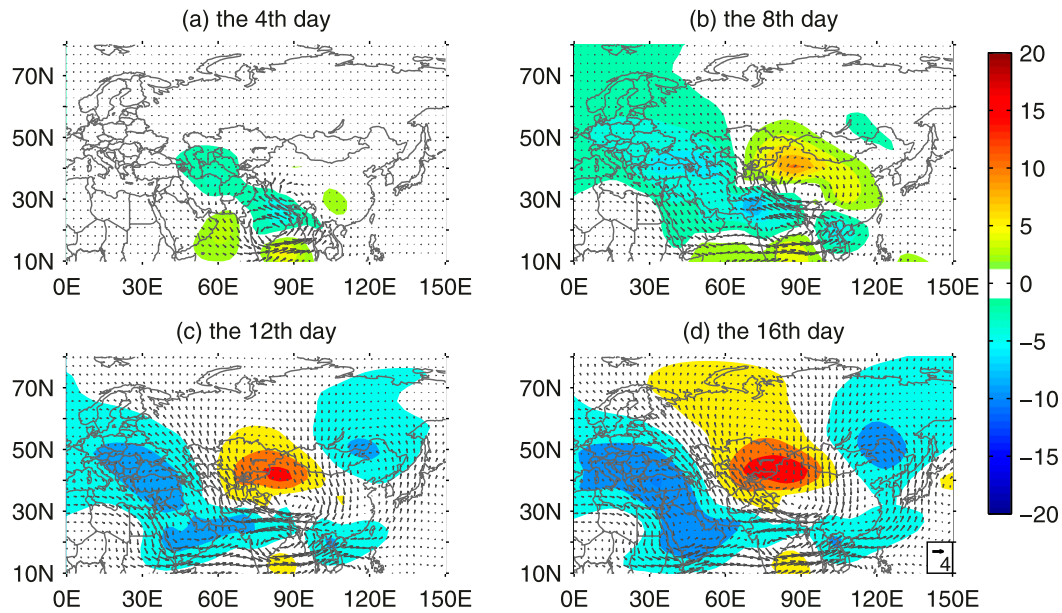


FIG. 10. Animated distribution of anomalous geopotential height and wind field evolution within 16 consecutive days of forcing with diabatic heating over the IS (center: 25°N, 80°E, horizontal scale: 20°E \times 10°N).

enhanced, which could enhance the $-+-$ PJ like pattern and thus form an IS–ICP–NC teleconnection.

4. Summary and discussion

Because of the interactive margin between the EASM and westerly, summer rainfall in northern China exhibits high variability. New mechanisms impacting summer rainfall variations in northern China are investigated.

Based on the high correlation of JA rainfall over the Indian subcontinent and northern China, this study investigates JA rainfall patterns and suggests a tripole pattern of the rainfall. By analyzing geostationary

satellite data from the *FY-2G* satellite and reanalysis data, we highlight that the distributions of circulation and vorticity indicate three teleconnections (see Fig. 11). The IS–ICP–NC teleconnection is suggested to be a significant pattern, and ISM-related convective heating enhances a PJ-like pattern through a Kelvin wave response and local Hadley circulation over the west Pacific at interannual and interdecadal time scales (Hu 1997; Wu et al. 2009). The IS–NC teleconnection links JA cyclones over the IS, troughs over NC, and anticyclones over the eastern Tibetan Plateau that could modulate summer rainfall over northern China. By comparing moisture fluxes and vertical velocities over

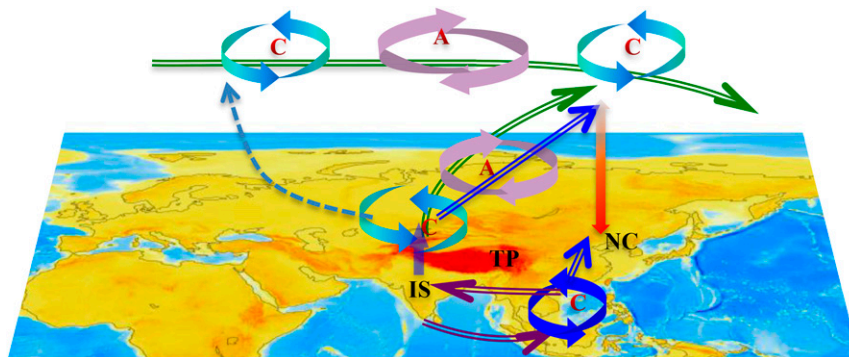


FIG. 11. Teleconnection (green arrow) and water vapor transport (blue arrow) in the mid-troposphere (500 hPa) and the relations to NC precipitation, as well as the linkage of IS and ICP circulation (pink arrow). The letters A and C indicate anticyclone and cyclone, respectively.

the western and southern profiles of NC, it is revealed that the IS–NC circulation could lead to mid- to upper-level moisture transport and effective rainfall with the deep ascending motion; in addition, moisture in NC could change moisture and vertical stability over NC. Enhancements in the ISM contributing anomalous convection heating could modulate the midlatitude Silk Road wave train via west-central Asia and NC, which further modulates NC circulation. To summarize, vorticity anomaly due to IS–ICP–NC and IS–NC teleconnections and the Silk Road wave train could change mid- to upper-level circulation, all of them resulting in an anomaly of ascending motion, which further changes the depth and efficient level of rainfall and makes a significant contribution to precipitation. In addition, PDO could explain the IS–ICP–NC pattern and PJ pattern at the multidecadal time scale due to the response of the SST pattern in the Indian and Pacific Ocean (Qian and Zhou 2014). The EASM and ICP–NC patterns are the primary factors for moisture transport over northern China and have relationships with the IS–NC pattern. Both of the IS–NC and ICP–NC patterns have inner linkages, cyclones, and moisture flux that could be transported toward the IS from the ICP and western Pacific on the southern side of the WPSH. The eastward moisture from IS to ICP along the southwesterly cross-equatorial flows could modulate ICP and Indo-Pacific moisture and circulation (see Fig. 11). In addition, EASM circulation could lead to lower-level moisture and effective rainfall with a relatively shallow effective level. The quantitative relationships of these results require further study.

The westward-extending WPSH, enhancing TP heating and IS cyclones are three possible factors contributing to the IS–NC teleconnection, and their variations are important for the IS–NC pathway. Simulation results show that enhancement in the IS cyclone corresponding to high diabatic heating could lead to an IS–NC circulation pattern, which in turn could modulate the tripole pattern of rainfall anomalies. Previous studies have shown that the eastward expansion of the South Asian high, due to increased thermal heating or decreased snow cover over the Tibetan Plateau (Zhang et al. 2018), could be responsible for the westward-extending WPSH. Therefore, the IS–NC variations due to thermal anomalies over the Tibetan Plateau require further discussion (Zhang et al. 2015). The links between IS cyclones and sea surface temperature and ENSO also require further exploration. To improve the simulation precision, local parameterization schemes and data observed from the third Tibetan Plateau experiment will be used as initial data (<http://tipex.data.cma.cn/tipex.html>; 2013–23) and be assimilated into the model

to improve simulation accuracy around the Tibetan Plateau.

The study uses HYSPLIT to explore moisture transport in the midtroposphere, and it can indicate midlevel moisture transport from IS to NC; however, the quantity evaluation of those moisture contributions to NC precipitation is worthy of further exploration using climate models.

Acknowledgments. This research was supported by the National Key R&D Program of China (Grant 2016YFA0600702), the National Natural Science Foundation of China for Key Program (Grant 41630426) and Distinguished Young Scientists (Grant 41625019), and the Qing Lan Project and Priority Academic Program Development of the Jiangsu Higher Education Institutions (PAPD). We thank the ECMWF for providing the ERA-Interim data (<http://apps.ecmwf.int/datasets/>), the GPCC and CRU monthly rainfall datasets, and the FY-2G data (<http://satellite.nsmc.org.cn/PortalSite/Data/>).

REFERENCES

- Ashok, K., Z. Guan, and T. Yamagata, 2001: Impact of the Indian Ocean dipole on the relationship between the Indian monsoon rainfall and ENSO. *Geophys. Res. Lett.*, **28**, 4499–4502, <https://doi.org/10.1029/2001GL013294>.
- Becker, A., P. Finger, A. Meyer-Christoffer, B. Rudolf, K. Schamm, U. Schneider, and M. Ziese, 2013: A description of the global land-surface precipitation data products of the Global Precipitation Climatology Centre with sample applications including centennial (trend) analysis from 1901–present. *Earth Syst. Sci. Data*, **5**, 71–99, <https://doi.org/10.5194/essdd-5-921-2012>.
- Dee, D. P., and Coauthors, 2011: The ERA-Interim re-analysis: Configuration and performance of the data assimilation system. *Quart. J. Roy. Meteor. Soc.*, **137**, 553–597, <https://doi.org/10.1002/qj.828>.
- Ding, Q., and B. Wang, 2005: Circumglobal teleconnection in the NH summer. *J. Climate*, **18**, 3483–3505, <https://doi.org/10.1175/JCLI3473.1>.
- Dong, W., and Coauthors, 2016: Summer rainfall over the southwestern Tibetan Plateau controlled by deep convection over the Indian subcontinent. *Nat. Commun.*, **7**, 10925, <https://doi.org/10.1038/ncomms10925>.
- Feng, L., and T. Zhou, 2012: Water vapor transport for summer rainfall over the Tibetan Plateau: Multi-dataset analysis. *J. Geophys. Res.*, **117**, D20114, <https://doi.org/10.1029/2011JD017012>.
- Gadgil, S., 2003: The Indian monsoon and its variability. *Annu. Rev. Earth Planet. Sci.*, **31**, 429–467, <https://doi.org/10.1146/annurev.earth.31.100901.141251>.
- Guo, Q., and J. Wang, 1988: A comparative study on summer monsoon in China and India. *J. Trop. Meteor.*, **4**, 53–60.
- Guo, Y., J. Cao, L. I. Hui, J. Wang, and Y. Ding, 2016: Simulation of the interface between the ISM and the East Asian summer monsoon: Intercomparison between MPI-ESM and ECHAM5/

- MPI-OM. *Adv. Atmos. Sci.*, **33**, 294–308, <https://doi.org/10.1007/s00376-015-5073-z>.
- Hsu, H.-H., and S.-M. Lin, 2007: Asymmetry of the tripole rainfall pattern during the East Asian summer. *J. Climate*, **20**, 4443–4458, <https://doi.org/10.1175/JCLI4246.1>.
- Hu, K., G. Huang, and R. Huang, 2011: The impact of tropical Indian Ocean variability on summer surface air temperature in China. *J. Climate*, **24**, 5365–5377, <https://doi.org/10.1175/2011JCLI4152.1>.
- Hu, Z., 1997: Interdecadal variability of summer climate over East Asia and its association with 500-hPa height and global sea surface temperature. *J. Geophys. Res.*, **102**, 19403–19412, <https://doi.org/10.1029/97JD01052>.
- Huang, W., S. Feng, J. H. Chen, and F. H. Chen, 2015a: Physical mechanisms of summer precipitation variations in the Tarim Basin in northwestern China. *J. Climate*, **28**, 3579–3591, <https://doi.org/10.1175/JCLI-D-14-00395.1>.
- , J. H. Chen, X. J. Zhang, S. Feng, and F. H. Chen, 2015b: Definition of the core zone of the “westerlies-dominated climatic regime”, and its controlling factors during the instrumental period. *Sci. China Earth Sci.*, **58**, 676–684, <https://doi.org/10.1007/s11430-015-5057-y>.
- , X. He, Z. Yang, T. Qiu, J. S. Wright, B. Wang, and D. Lin, 2018: Moisture sources for wintertime extreme precipitation events over South China during 1979–2013. *J. Geophys. Res. Atmos.*, **123**, 6690–6712, <https://doi.org/10.1029/2018jd028485>.
- Jiang, X., and M. Ting, 2017: A dipole pattern of summertime rainfall across the Indian subcontinent and the Tibetan Plateau. *J. Climate*, **30**, 9607–9620, <https://doi.org/10.1175/JCLI-D-16-0914.1>.
- Kripalani, R., and A. Kulkarni, 1997: Rainfall variability over South-east Asia—Connections with Indian monsoon and ENSO extremes: New perspectives. *Int. J. Climatol.*, **17**, 1155–1168, [https://doi.org/10.1002/\(SICI\)1097-0088\(199709\)17:11<1155::AID-JOC188>3.0.CO;2-B](https://doi.org/10.1002/(SICI)1097-0088(199709)17:11<1155::AID-JOC188>3.0.CO;2-B).
- , and —, 2001: Monsoon rainfall variations and teleconnections over South and East Asia. *Int. J. Climatol.*, **21**, 603–616, <https://doi.org/10.1002/joc.625>.
- , —, and S. Singh, 1997: Association of the ISM with the Northern Hemisphere mid-latitude circulation. *Int. J. Climatol.*, **17**, 1055–1067, [https://doi.org/10.1002/\(SICI\)1097-0088\(199708\)17:10<1055::AID-JOC180>3.0.CO;2-3](https://doi.org/10.1002/(SICI)1097-0088(199708)17:10<1055::AID-JOC180>3.0.CO;2-3).
- Krishnan, R., and M. Sugi, 2001: Baiu rainfall variability and associated monsoon teleconnections. *J. Meteor. Soc. Japan*, **79**, 851–860, <https://doi.org/10.2151/jmsj.79.851>.
- Li, C. F., and M. Yanai, 1996: The onset and interannual variability of the Asian summer monsoon in relation to land–sea thermal contrast. *J. Climate*, **9**, 358–375, [https://doi.org/10.1175/1520-0442\(1996\)009<0358:TOAIVO>2.0.CO;2](https://doi.org/10.1175/1520-0442(1996)009<0358:TOAIVO>2.0.CO;2).
- Li, C. Y., J. Pan, and Z. P. Que, 2011: Variation of the East Asian Monsoon and the tropospheric biennial oscillation. *Chin. Sci. Bull.*, **56**, 70–75, <https://doi.org/10.1007/s11434-010-4200-6>.
- Li, J., D. Li, and J. Zhang, 2012: Research on summer effective precipitation conversion rate over the Yellow River basin (in Chinese). *Shui Kexue Jinzhan*, **23**, 346–354.
- Liu, H., S. Tang, J. Hu, S. Zhang, and X. Deng, 2017: An improved physical split-window algorithm for precipitable water vapor retrieval exploiting the water vapor channel observations. *Remote Sens. Environ.*, **194**, 366–378, <https://doi.org/10.1016/j.rse.2017.03.031>.
- Liu, Y., and Y. Ding, 2008: Analysis and numerical simulation of the teleconnection between ISM and precipitation in North China. *Acta Meteor. Sin.*, **66**, 789–799, <https://doi.org/10.11676/qxxb2008.072>.
- Nitta, T., 1987: Convective activities in the tropical western Pacific and their impact on the Northern Hemisphere summer circulation. *J. Meteor. Soc. Japan*, **65**, 373–390, https://doi.org/10.2151/jmsj1965.65.3_373.
- Qian, C., and T. Zhou, 2014: Multidecadal variability of North China aridity and its relationship to PDO during 1900–2010. *J. Climate*, **27**, 1210–1222, <https://doi.org/10.1175/JCLI-D-13-00235.1>.
- Qian, W. H., X. L. Shan, D. L. Chen, C. W. Zhu, and Y. F. Zhu, 2012: Drought near the northern fringe of the East Asian summer monsoon in China during 1470–2003. *Climatic Change*, **110**, 373–383, <https://doi.org/10.1007/s10584-011-0096-7>.
- Sodemann, H., C. Schwierz, and H. Wernli, 2008: Interannual variability of Greenland winter precipitation sources: Lagrangian moisture diagnostic and North Atlantic Oscillation influence. *J. Geophys. Res.*, **113**, D03107, <https://doi.org/10.1029/2007JD008503>.
- Stein, A. F., R. R. Draxler, G. D. Rolph, B. J. B. Stunder, M. D. Cohen, and F. Ngan, 2015: NOAA’s HYSPLIT atmospheric transport and dispersion modeling system. *Bull. Amer. Meteor. Soc.*, **96**, 2059–2077, <https://doi.org/10.1175/BAMS-D-14-00110.1>.
- Takaya, K., and H. Nakamura, 2001: A formulation of a phase-independent wave-activity flux for stationary and migratory quasigeostrophic eddies on a zonally varying basic flow. *J. Atmos. Sci.*, **58**, 608–627, [https://doi.org/10.1175/1520-0469\(2001\)058<0608:AFOAPI>2.0.CO;2](https://doi.org/10.1175/1520-0469(2001)058<0608:AFOAPI>2.0.CO;2).
- Tao, S., and L. Chen, 1987: A review of recent research on the East Asian summer monsoon in China. *Monsoon Meteorology*, C. P. Chang and T. N. Krishnamurti, Eds., Oxford University Press, 60–92.
- Wang, B., B. Xiang, J. Li, P. J. Webster, M. N. Rajeevan, J. Liu, and K.-J. Ha, 2015: Rethinking Indian monsoon rainfall prediction in the context of recent global warming. *Nat. Commun.*, **6**, 7154, <https://doi.org/10.1038/ncomms8154>.
- Wang, C., and J. Huang, 2006: The instability of the remote relationship between North China and Indian summer rainfall (in Chinese). *Prog. Nat. Sci.*, **16**, 981–985.
- Wang, D., and A. Wang, 2017: Applicability assessment of GPCP and CRU precipitation products in China during 1901 to 2013 (in Chinese). *Climatic Environ. Res.*, **22**, 446–462.
- Watanabe, M., and M. Kimoto, 2000: Atmosphere–ocean thermal coupling in the North Atlantic: A positive feedback. *Quart. J. Roy. Meteor. Soc.*, **126**, 3343–3369, <https://doi.org/10.1002/qj.49712657017>.
- Wu, B., and T. Zhou, 2008: Oceanic origin of the interannual and interdecadal variability of the summertime western Pacific subtropical high. *Geophys. Res. Lett.*, **35**, L13701, <https://doi.org/10.1029/2008GL034584>.
- , —, and T. Li, 2009: Seasonally evolving dominant interannual variability modes of East Asian climate. *J. Climate*, **22**, 2992–3005, <https://doi.org/10.1175/2008JCLI2710.1>.
- Wu, G., Y. Liu, B. He, Q. Bao, A. Duan, and F. F. Jin, 2012: Thermal controls on the Asian summer monsoon. *Sci. Rep.*, **2**, 404, <https://doi.org/10.1038/srep00404>.
- Wu, Z., and N. E. Huang, 2009: Ensemble empirical mode decomposition: A noise-assisted data analysis method. *Adapt. Data Anal.*, **1**, 1–41, <https://doi.org/10.1142/S1793536909000047>.

- Xu, X., C. Lu, X. Shi, and S. Gao, 2008: World water tower: An atmospheric perspective. *Geophys. Res. Lett.*, **35**, L20815, <https://doi.org/10.1029/2008GL035867>.
- Yang, J., Q. Liu, Z. Liu, L. Wu, and F. Huang, 2009: Basin mode of Indian Ocean sea surface temperature and Northern Hemisphere circunglobal teleconnection. *Geophys. Res. Lett.*, **36**, L19705, <https://doi.org/10.1029/2009GL039559>.
- Yang, L., Z. H. Wang, Y. L. Chu, H. Zhao, and M. Tang, 2014: Water vapor motion signal extraction from FY-2E long-wave IR infrared window imagery images for cloud-free regions: The temporal difference technique. *Adv. Atmos. Sci.*, **31**, 1386–1394, <https://doi.org/10.1007/s00376-014-3165-9>.
- Zhang, J., S. Gao, H. Chen, J. Yu, and Q. Tang, 2015: Retrieval of the land surface–air temperature difference from high spatial resolution satellite observations over complex surfaces in the Tibetan Plateau. *J. Geophys. Res. Atmos.*, **120**, 8065–8079, <https://doi.org/10.1002/2015JD023395>.
- , C. Liu, and H. Chen, 2018: The modulation of Tibetan Plateau heating on the multi-scale northernmost margin activity of East Asia summer monsoon in northern China. *Global Planet. Change*, **161**, 149–161, <https://doi.org/10.1016/j.gloplacha.2017.12.011>.
- , H. Chen, and Q. Zhang, 2019: Extreme drought in the recent two decades in northern China resulting from Eurasian warming. *Climate Dyn.*, **52**, 2885–2902, <https://doi.org/10.1007/s00382-018-4312-2>.
- Zhang, R., 2001: Relations of water vapor transport from Indian monsoon with that over East Asia and summer rainfall in China. *Adv. Atmos. Sci.*, **18**, 1005–1007, <https://doi.org/10.1007/BF03403519>.
- Zhou, L., H. Zou, S. Ma, F. Li, J. Zhu, P. Li, and Y. Zhang, 2016: The observed impacts of South Asian summer monsoon on the local atmosphere and the near-surface turbulent heat exchange over the Southeast Tibet. *J. Geophys. Res. Atmos.*, **120**, 11 509–11 518, <https://doi.org/10.1002/2014jd022928>.
- Zhu, X., Y. Liu, and G. Wu, 2012: An assessment of summer sensible heat flux on the Tibetan Plateau from eight datasets. *Sci. China Earth Sci.*, **55**, 779–786, <https://doi.org/10.1007/s11430-012-4379-2>.